Thermodynamic Performance Enhancement and NOx Emission Assessment in a Triple-Spool Turbofan Engine with an Interstage Turbine Burner

Raed Kafafy *

Posted Date: 18 May 2026

doi: 10.20944/preprints202605.1093.v1

Keywords: interstage turbine burner; triple-spool turbofan; thermodynamic cycle analysis; NOx emissions; aircraft gas turbine; specific thrust; thrust specific fuel consumption; separate-exhaust turbofan

 doi:10.20944/preprints202605.1093.v1

Article

Thermodynamic Performance Enhancement and NOx Emission Assessment in a Triple-Spool Turbofan Engine with an Interstage Turbine Burner

Raed Kafafy

Engineering Technology and Science, Higher Colleges of Technology, Al Ain, United Arab Emirates; rkafafy@hct.ac.ae

Abstract

The increasing demand for higher efficiency and lower emissions in aircraft gas turbines motivates investigation of alternative thermodynamic cycle architectures. This study assesses the performance and NOx emission behavior of a triple-spool, separate-exhaust turbofan engine equipped with an interstage turbine burner (ITB). A baseline engine representative of the RB211 Trent 892 is first modeled and verified against publicly available takeoff reference data. The cycle is then modified by introducing an isobaric secondary combustion process between the high-pressure and intermediate-pressure turbines. The effects of fan pressure ratio, bypass ratio, overall pressure ratio, high-pressure turbine inlet temperature, and ITB exit temperature are examined using two-parameter response-surface sweeps. Main-combustor NOx is estimated using an RQL-type cycle correlation, while the ITB contribution is represented using an engineering source–sink model accounting for new NOx formation and partial reburning of upstream NOx. The baseline model predicts specific thrust, TSFC, and EINOx within ±8% of reference values. At a selected ITB operating point, specific thrust increases by 1.98%, TSFC increases by 9.84%, thermal efficiency decreases by 2.56%, and the adopted engineering source–sink model predicts a 20.03% reduction in fuel-flow-weighted EINOx.

Keywords: interstage turbine burner; triple-spool turbofan; thermodynamic cycle analysis; NOx emissions; aircraft gas turbine; specific thrust; thrust specific fuel consumption; separate-exhaust turbofan

1. Introduction

Turbofan engines for aviation propulsion have undergone major improvements over the past several decades through advances in compressor pressure ratio, turbine inlet temperature, component efficiency, turbine cooling, materials, and fan bypass ratio [1,2]. These developments have substantially reduced fuel consumption per passenger-kilometer and enabled modern turbofan engines to achieve high levels of thermal and propulsive efficiency. Nevertheless, the continued growth of air traffic and the increasing emphasis on environmental sustainability place additional pressure on engine designers to further improve fuel efficiency while reducing pollutant emissions, particularly nitrogen oxides (NOx) [3–5].

In conventional gas-turbine engines, thermal efficiency is commonly improved by increasing the overall pressure ratio and the turbine inlet temperature. However, this approach introduces important thermodynamic and environmental trade-offs. Higher turbine inlet temperatures generally increase the need for turbine cooling, which can reduce cycle efficiency because a portion of the compressed air bypasses the main combustion process. At the same time, higher combustor pressure and temperature tend to increase thermal NOx formation [6,7]. Recent NOx-emission studies based on operational engine data also confirm that overall pressure ratio, thrust, fuel flow, and combustor technology strongly influence NOx prediction, and that low fuel burn is often associated with higher pressure ratios and increased NOx tendency [7]. Therefore, future engine

 doi:10.20944/preprints202605.1093.v1

architectures require strategies that can improve performance without relying exclusively on further increases in main combustor exit temperature.

One such strategy is to redistribute heat addition within the cycle by introducing combustion during or between turbine expansion processes. Sirignano and Liu [8] proposed the interstage turbine burner (ITB) concept, in which combustion is continued inside the turbine to improve specific thrust and cycle efficiency. Liu and Sirignano [9] later extended the concept to turbojet and turbofan engines and considered discrete interstage turbine burners as an intermediate configuration between conventional combustion and continuous turbine burning. Multiple interstage-burner arrangements have also been investigated, showing that their benefits depend strongly on cooling requirements, application type, and heat-addition distribution [10]. These studies established the thermodynamic potential of turbine burning while also indicating that practical advantages must be assessed together with cooling, pressure loss, combustor integration, and turbine durability.

Several studies have examined ITB-equipped engines from a cycle-analysis perspective. Liew et al. [11] performed a parametric cycle analysis of a dual-spool, separate-exhaust turbofan engine with an ITB located between the high-pressure and low-pressure turbines. Their results indicated that ITB integration can increase specific thrust, reduce cooling-air requirements, and possibly reduce NOx production when the main burner and ITB exit temperatures are properly selected. Subsequent studies extended the analysis to on-design and off-design operation of separate-exhaust turbofan engines with ITB, showing that the concept can influence specific thrust, thrust specific fuel consumption, and engine operating characteristics across different flight conditions and throttle settings [12–14]. Later studies examined structural and dimensional implications of adding an inter-turbine combustor to a turbofan engine, highlighting that ITB integration affects not only thermodynamic performance but also component sizing and engine layout [15].

More recent studies have renewed interest in ITB architectures because of their potential relevance to future very-high-bypass-ratio and ultra-high-bypass-ratio engines. Yin and Rao [16] investigated an ITB applied to a next-generation aero-engine and reported that the concept can substantially reduce high-pressure turbine cooling requirements and lower NOx emissions without penalizing specific fuel consumption under selected conditions. Their later review emphasized that ITB engines may offer benefits for sustainability, fuel flexibility, and future energy-mix strategies, but also identified unresolved issues related to combustor design, emissions, operability, turbine durability, and technology readiness [17]. Recent work on turbine internal burner technology has also shown potential thermal-performance improvements with negligible TSFC increment, although the concept remains largely at the theoretical and computational development stage [18].

The ITB concept has also been explored in advanced propulsion and energy architectures. Ji et al. [19] proposed a turbojet engine integrated with both an ITB and a solid oxide fuel cell for more/all-electric aircraft applications, showing improvements in thermal efficiency and specific thrust compared with a conventional turbojet configuration. Although such hybrid configurations differ from the present turbofan architecture, they demonstrate the broader relevance of ITB concepts beyond conventional thrust augmentation. In parallel, numerical and experimental studies of ultra-compact combustors have explored possible physical implementations of ITB systems. Conrad [20] examined inter-turbine-burner integration in a small jet turbine engine facility, while Zhang et al. [21] investigated an ultra-compact ITB with a trapped-vortex slot inlet. These studies indicate that practical ITB implementation depends on combustor stability, mixing, pressure loss, outlet temperature uniformity, fuel injection, and integration with turbine hardware.

Despite these promising findings, the performance and emissions implications of ITB remain dependent on engine architecture, operating conditions, and modeling assumptions. A central point of uncertainty is whether the additional combustion introduced by an ITB reduces or increases overall NOx emissions. On one hand, shifting part of the heat addition downstream of the high-pressure turbine can reduce the required main combustor exit temperature and high-pressure turbine thermal loading, which may reduce thermal NOx formation. On the other hand, the ITB itself introduces an additional combustion zone, and its contribution to total NOx depends on local temperature,

 doi:10.20944/preprints202605.1093.v1

pressure, equivalence ratio, residence time, and mixing quality. Generic aero-engine emission-prediction methods and combustor-specific NOx correlations are therefore important when evaluating nonconventional cycles, particularly when detailed proprietary combustor data are unavailable [22]. Data-driven NOx studies also show that combustor-specific models provide more reliable predictions than general correlations, supporting a cautious interpretation of NOx trends in simplified cycle analysis [7].

Most published ITB studies have focused on turbojet, dual-spool turbofan, two-spool separate-exhaust turbofan, or ultra-high-bypass-ratio engine configurations. By comparison, fewer studies have addressed triple-spool separate-exhaust turbofan engines, despite their practical relevance to modern large aero-engines. A triple-spool architecture introduces additional design flexibility because the fan, intermediate-pressure compressor, and high-pressure compressor are driven by separate turbine systems. This affects the distribution of turbine work, component pressure ratios, bypass ratio, and the possible placement and thermodynamic influence of an ITB. A recent study by Kafafy and Ravichandran [23] examined the parametric cycle performance of a triple-spool, separate-exhaust turbofan engine with an interstage turbine burner located between the high-pressure turbine and the intermediate-pressure turbine. The present work extends that earlier analysis by explicitly coupling the thermodynamic performance assessment with NOx emission trends, thereby emphasizing the trade-off between performance enhancement and environmental impact.

The aim of this study is to assess the thermodynamic performance and NOx emission behavior of a triple-spool, separate-exhaust turbofan engine equipped with an ITB. A conventional triple-spool turbofan engine is first modeled as the baseline configuration. The cycle is then modified by introducing an isobaric ITB, and the effects of fan pressure ratio, bypass ratio, overall compressor pressure ratio, high-pressure turbine inlet temperature, and ITB exit temperature are examined parametrically. The main contributions of the present study are fourfold. First, a variable-property thermodynamic cycle model is developed for a triple-spool, separate-exhaust turbofan engine with optional ITB heat addition and simplified turbine cooling. Second, the baseline model is verified against publicly available Trent 892 takeoff performance and emissions data. Third, two-parameter response-surface sweeps are used to examine the effects of FPR–BPR, OPR–HPTIT, and HPTIT–IPTIT on specific thrust, TSFC, thermal efficiency, and EINOx. Fourth, an engineering ITB source–sink NOx model is introduced to estimate comparative ITB emission trends by accounting for new NOx formation and partial reburning of upstream main-combustor NOx.

2. Thermodynamic and Emissions Modelling Framework

2.1. Engine Configurations and Station Numbering

The present study considers two triple-spool, separate-exhaust turbofan configurations: a baseline engine and a modified engine incorporating an interstage turbine burner (ITB). The baseline configuration represents a conventional high-bypass civil turbofan with separate exhausts. In this engine, the fan is driven by the low-pressure turbine (LPT), the intermediate-pressure compressor (IPC) is driven by the intermediate-pressure turbine (IPT), and the high-pressure compressor (HPC) is driven by the high-pressure turbine (HPT). The three spools are mechanically independent and may therefore rotate at different shaft speeds, providing additional flexibility in compressor-turbine matching compared with two-spool architectures [24–26]. In the baseline engine, the core stream passes successively through the inlet, fan, IPC, HPC, main combustor, HPT, IPT, LPT, and core nozzle, while the bypass stream passes through the inlet, fan, bypass duct, and fan nozzle.

The modified configuration is derived from the baseline engine by inserting an ITB between the HPT and the IPT, as shown schematically in Figure 1. The main combustor remains located between the HPC and the HPT, while the ITB introduces a second heat-addition process downstream of the HPT. Accordingly, in the modified engine, the core stream passes through the inlet, fan, IPC, HPC, main combustor, HPT, ITB, IPT, LPT, and core nozzle. The bypass stream is unchanged and continues to expand separately through the fan nozzle. The ITB is modelled as an isobaric secondary combustor

 doi:10.20944/preprints202605.1093.v1

with prescribed combustion efficiency and total-pressure loss. Its role in the cycle model is to redistribute part of the total heat addition from the main combustor to a downstream location in the turbine system, thereby modifying the turbine temperature distribution, spool work balance, exhaust conditions, and emissions behavior.

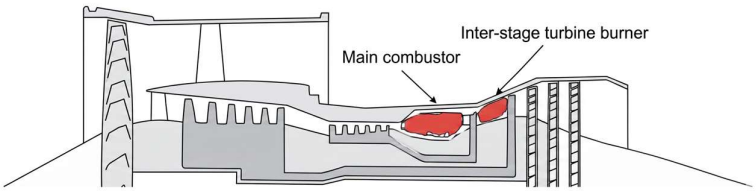

Figure 1. Schematic layout of the triple-spool, separate-exhaust turbofan engine with an interstage turbine burner. The main burner is located between the high-pressure compressor and high-pressure turbine, while the interstage turbine burner is located between the high-pressure turbine and intermediate-pressure turbine.

To enable direct comparison between the baseline and ITB configurations, a common station-numbering system is used throughout the cycle analysis. The station numbers identify the thermodynamic states at the inlet and exit of each major component and provide the basis for applying the component energy balances, pressure-loss relations, performance calculations, and NOx emission correlations. The station-numbering layout used for the baseline engine cycle is shown in Figure 2, whereas the station-numbering layout used for the modified engine cycle is shown in Figure 3.

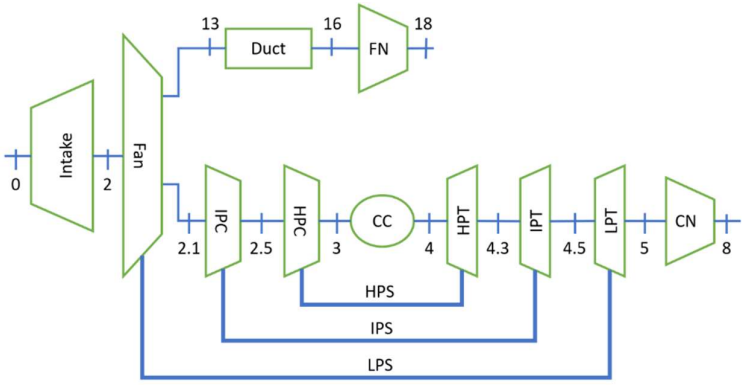

Figure 2. Layout and station numbering for the baseline triple-spool turbofan.

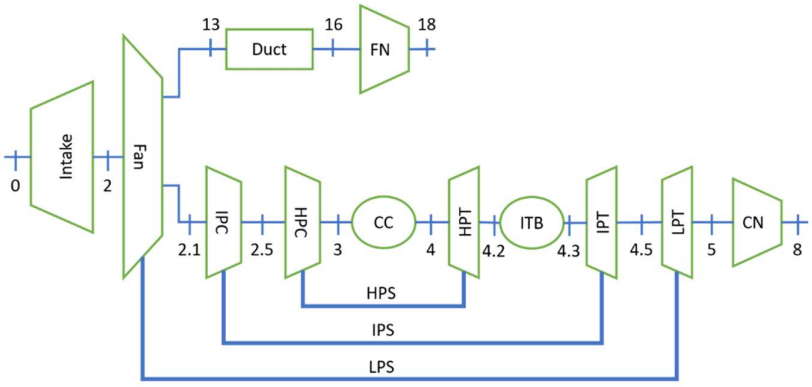

Figure 3. Layout and station numbering for the modified triple-spool turbofan with an interstage turbine burner.

 doi:10.20944/preprints202605.1093.v1

In the baseline engine, the HPT exit and IPT inlet are represented by a single station. In the modified configuration, this location is split by the insertion of the ITB: station 4.2 is assigned to the HPT exit/ITB inlet, and station 4.3 is assigned to the ITB exit/IPT inlet. This allows the ITB inlet and exit conditions to be evaluated explicitly while preserving the overall numbering logic of the baseline engine. The station definitions used for the baseline configuration are summarized in Table 1. The additional or modified station definitions introduced by the ITB configuration are summarized in Table 2.

Table 1. Station definitions for the baseline triple-spool turbofan engine.

Stn	Location	Stn	Location
0	Freestream / atmospheric condition	4.3	HPT exit / IPT entry
1	Intake entry	4.5	IPT exit / LPT entry
2	Intake exit / fan entry	5	LPT exit / core nozzle entry
2.1	Fan core exit / IPC entry	8	Core nozzle exit
2.5	IPC exit / HPC entry	13	Fan bypass exit / bypass duct entry
3	HPC exit / main combustor entry	16	Fan duct exit / fan nozzle entry
4	Main combustor exit / HPT entry	18	Fan nozzle exit

Table 2. Additional or modified station definitions for the ITB engine.

Stn	Location
4.2	HPT exit / ITB entry
4.3	ITB exit / IPT entry
4.5	IPT exit / LPT entry

2.2. Thermodynamic Cycle Model

The baseline engine selected in this study approximates the Rolls-Royce RB211 Trent 892-17 series, which belongs to Trent 800 family of high-bypass, triple-spool, separate-exhaust turbofan engines. The engine identity and architecture are supported by the EASA type-certificate data sheet for the RB211 Trent 800 series [27], while the numerical cycle and emissions inputs used in the present analysis are taken from the ICAO emissions databank entry for Trent 892 [28]. The baseline specifications and performance parameters at the studied operating condition are summarized in Table 3. These data correspond to the maximum-takeoff, sea-level static, standard-atmosphere condition. In Table 3, RPM denotes shaft rotational speed in revolutions per minute, OPR denotes the overall pressure ratio, defined as the total pressure downstream of the HPC divided by the total pressure upstream of the fan, and TSFC denotes thrust-specific fuel consumption, defined as the fuel mass flow rate divided by engine net thrust. The same baseline specifications are applied to the ITB-modified configuration to ensure that the comparison isolates the effect of introducing the interstage turbine burner rather than changes in the reference engine data.

 doi:10.20944/preprints202605.1093.v1

Table 3. Baseline engine specifications and rated performance parameters at maximum-takeoff, sea-level static, ISA conditions.

Specifications		Performance at maximum takeoff, sea-level static, ISA condition	
Model/Variant	RB211 Trent 892-17	**RPM (%)**	100.5% (HPS) 105.0% (IPS) 100.5% (LPS)
Manufacturer	Rolls-Royce Deutschland Ltd. & Co KG	**RPM (100%)**	10,611 (HPS) 7,000 (IPS) 3,300 (LPS)
Aircraft application	Boeing 777-200ER, 777-300	**Bypass ratio**	5.7:1
Compressor	1-stage fan, 8-stage IPC, 6-stage HPC	**Overall Pressure ratio (OPR)**	41.4:1
Combustor	Single Annular (24 nozzles)	**Mass flowrate**	1,200 kg/s (2,645.5 lb/s)
Turbine	1-stage HPT, 1-stage IPT, 5-stage LPT	**Net thrust**	411.5 kN (92,509 lbf)
		TSFC	9.50 mg/(N.s) (0.335 lb/(lbf·h))

*__Note__: HPS, IPS, and LPS denote the high-pressure, intermediate-pressure, and low-pressure spools, respectively. IPC, HPC, HPT, IPT, and LPT denote the intermediate-pressure compressor, high-pressure compressor, high-pressure turbine, intermediate-pressure turbine, and low-pressure turbine, respectively. Data are representative of the RB211 Trent 892-17 at maximum-takeoff, sea-level static, ISA conditions [27,28].

To account for variations in gas properties at elevated temperatures, the thermodynamic model employs a variable-specific-heat formulation in which the specific heats are functions of temperature and local fuel-air ratio. Specific enthalpy is evaluated using fourth-order polynomial fits derived from NASA chemical-equilibrium and thermodynamic-property data [29–31]. The gas properties are obtained by interpolating between dry-air properties and combustion-product properties according to the local fuel-air ratio. This approach avoids constant-property assumptions and allows the component energy balances to be formulated in terms of enthalpy. It therefore improves the consistency of the calculated compressor work, turbine power, main-combustor fuel-air ratio, ITB fuel-air ratio, and nozzle expansion properties, particularly at the elevated temperatures encountered downstream of the main combustor and ITB.

The same component modelling assumptions are used for the baseline and ITB-modified configurations unless otherwise stated. The inlet, fan, compressors, turbines, ducts, combustors, and nozzles are modelled as steady-flow components. The flow at each engine station is represented by one-dimensional, area-averaged total temperature, total pressure, enthalpy, and fuel-air ratio. The fan, IPC, HPC, HPT, IPT, and LPT are modelled using prescribed polytropic efficiencies, while the mechanical power transfer between each turbine and its corresponding compressor or fan is corrected using shaft mechanical efficiency. Kinetic-energy changes inside the compressors, turbines, ducts, and combustors are neglected, except in the nozzle expansion calculations. Heat transfer to the surroundings is neglected for the turbomachinery, ducts, and nozzles.

The flight condition, component efficiencies, pressure losses, design-cycle parameters, and fuel lower heating value used in the thermodynamic cycle model are summarized in Table 4.

.

 doi:10.20944/preprints202605.1093.v1

Table 4. Flight condition, component efficiencies, pressure losses, design-cycle parameters, and fuel properties used in the thermodynamic cycle model.

Flight Condition		**Component Pressure Losses**	
Altitude, $\boldsymbol{h}$	0	Intake	1.0%
Mach number, $\boldsymbol{M_0}$	0	Main combustor	4.0%
Component Efficiencies		Interstage turbine burner	4.0%
Fan polytropic efficiency	92.0%	Core nozzle	1.0%
IPC polytropic efficiency	91.0%	Bypass nozzle and fan duct	1.0%
HPC polytropic efficiency	90.0%	**Design Cycle Parameters**	
HPT polytropic efficiency	89.0%	Bypass ratio	5.7
IPT polytropic efficiency	90.0%	Fan pressure ratio	1.68
LPT polytropic efficiency	92.0%	Overall pressure ratio	41.4
Main combustor efficiency	99.0%	HPT inlet temperature	1,740 K
ITB combustion efficiency	99.0%	**Fuel properties**	
Spools mechanical efficiency	99.0%	Lower heating value	43 MJ/kg

*__Note__: Component efficiencies, pressure losses, nozzle parameters, and fuel properties are modelling assumptions selected from standard gas-turbine cycle-analysis practice [25,26]. The ITB efficiency and pressure-loss assumptions are applied only to the ITB-modified configuration.

A simplified turbine cooling model is also included to account for the effect of blade-cooling air at elevated turbine inlet temperatures. The cooling fraction is prescribed as a function of the corresponding turbine inlet total temperature. No cooling is applied below a threshold temperature, while the cooling fraction increases with turbine inlet temperature up to a specified maximum value. For the baseline engine, the cooling model is applied to the HPT using the main-combustor exit total temperature and to the IPT using the HPT-exit/IPT-inlet total temperature. For the ITB-modified configuration, the HPT cooling fraction is based on T_{t4}, while the IPT cooling fraction is based on the ITB exit total temperature, $T_{t4.3}$. The extracted cooling air is mixed with the hot gas before the corresponding turbine expansion, thereby modifying the effective turbine inlet temperature and mass flow used in the turbine work balance. The cooling model uses a threshold temperature of 1300 K, a reference temperature of 1740 K, a reference cooling fraction of 6%, and a maximum cooling fraction of 12%.

The thermodynamic cycle model calculates the total temperature, total pressure, enthalpy, fuel-air ratio, mass flow rate, shaft work, nozzle exit velocity, net thrust, specific thrust, and thrust-specific fuel consumption at the engine stations defined in Section 2.1. The model is implemented as a station-by-station steady-flow calculation. For each component, the exit state is calculated from the inlet state, prescribed pressure ratio or pressure loss, component efficiency, and the appropriate energy balance. The exit total pressure for a compression component, being a fan, IPC, or HPC, is calculated from

$$P_{t,out} = \pi_c P_{t,in} \tag{1}$$

where π_c denotes the pressure ratio of the corresponding compression component. The outlet total temperature is calculated using the polytropic-efficiency relation,

$$T_{t,out} = T_{t,in}\left(\pi_c^{\frac{\gamma-1}{\gamma\eta_{p,c}}}\right) \tag{2}$$

where $\eta_{p,c}$ is the compressor or fan polytropic efficiency and γ is evaluated from the local gas properties. Because temperature-dependent gas properties are used, this relation is applied

 doi:10.20944/preprints202605.1093.v1

iteratively with the enthalpy calculation until the exit state is converged. The specific work of each compression component is then evaluated from the enthalpy rise,

$$w_c = h_{t,out} - h_{t,in} \tag{3}$$

where $h_{t,in}$ and $h_{t,out}$ are the inlet and outlet total specific enthalpies, respectively.

For the triple-spool configuration, the compressor and fan work requirements are evaluated separately. The HPC specific work is

$$w_{HPC} = h_{t3} - h_{t2.5}, \tag{4}$$

the IPC specific work is

$$w_{IPC} = h_{t2.5} - h_{t2.1}, \tag{5}$$

and the fan work per unit core air flow is

$$w_F = (1 + \alpha)(h_{t13} - h_{t2}) \tag{6}$$

where α is the bypass ratio (ratio of bypass mass flow rate to core mass flow rate). The factor $1 + \alpha$ accounts for the fact that the fan processes both the core and bypass streams.

The main combustor is modelled as a constant-pressure heat-addition component with a

$$P_{t4} = P_{t3}\left(1 - \frac{\Delta P_b}{P_{t3}}\right) \tag{7}$$

prescribed total-pressure loss. The combustor exit total pressure is

and the main-combustor fuel-air ratio is obtained from the steady-flow energy balance,

$$f_b = \frac{h_{t4} - h_{t3}}{\eta_b LHV - h_{t4}} \tag{8}$$

where f_b is the main-combustor fuel-air ratio, η_b is the main-combustor efficiency, and LHV is the fuel lower heating value.

The turbine temperature drops are determined from the spool power balances. In the baseline engine, the HPT drives the HPC, the IPT drives the IPC, and the LPT drives the fan. Therefore, the turbine enthalpy drops are calculated from

$$(1 + f_b)(h_{t4} - h_{t4.3})\eta_{m,HPS} = w_{HPC} \tag{9}$$

$$(1 + f_b)(h_{t4.3} - h_{t4.5})\eta_{m,IPS} = w_{IPC} \tag{10}$$

$$(1 + f_b)(h_{t4.5} - h_{t5})\eta_{m,LPS} = w_F \tag{11}$$

where $\eta_{m,HPS}$, $\eta_{m,IPS}$, $\eta_{m,LPS}$ are the mechanical efficiencies of the high-, intermediate-, and low-pressure spools. These equations define the HPT, IPT, and LPT exit enthalpies for the baseline configuration.

For the ITB-modified configuration, the HPT exit is station 4.2 rather than station 4.3. The HPT power balance becomes

$$(1 + f_b)(h_{t4} - h_{t4.2})\eta_{m,\mathrm{HPS}} = w_{HPC} \tag{12}$$

The ITB is then modelled as a second constant-pressure heat-addition component with its exit total pressure calculated from

$$P_{t4.3} = P_{t4.2}\left(1 - \frac{\Delta P_{ITB}}{P_{t4.2}}\right) \tag{13}$$

and its fuel-air ratio calculated from

$$f_{ITB} = \frac{(1 + f_b)(h_{t4.3} - h_{t4.2})}{\eta_{ITB} LHV - h_{t4.3}} \tag{14}$$

 doi:10.20944/preprints202605.1093.v1

where f_{ITB} is the ITB fuel-air ratio and η_{ITB} is the ITB combustion efficiency. Downstream of the ITB, the total fuel-air ratio is

$$f_{tot} = f_b + f_{ITB} \tag{15}$$

The IPT and LPT power balances for the ITB-modified engine are then written as

$$(1 + f_{tot})(h_{t4.3} - h_{t4.5})\eta_{m,\mathrm{IPS}} = w_{IPC} \tag{16}$$

$$(1 + f_{tot})(h_{t4.5} - h_{t5})\eta_{m,LPS} = w_F \tag{17}$$

The core and bypass streams are expanded through separate nozzles. For each nozzle, choking is assessed using the local total-to-ambient pressure ratio. If the nozzle is unchoked, the exit static pressure is set equal to the ambient pressure. If the nozzle is choked, the exit Mach number is set to unity and the exit static pressure is determined from the critical pressure ratio. The nozzle exit velocity is calculated from the total-to-static enthalpy drop,

$$V_e = \sqrt{2\eta_n\left(h_{t,in} - h_e\right)} \tag{18}$$

where η_n is the nozzle efficiency, $h_{t,in}$ is the nozzle-inlet total enthalpy, and h_e is the nozzle-exit static enthalpy.

The net thrust of the separate-exhaust turbofan is obtained by summing the core and bypass thrust contributions,

$$F_N = \dot{m}_c[(1 + f_{tot})V_8 - V_0] + (P_8 - P_0)A_8 + \alpha\dot{m}_c(V_{18} - V_0) + (P_{18} - P_0)A_{18} \tag{19}$$

where F_N is the net thrust, $\dot{m}_c$ is the core air mass flow rate, α is the bypass ratio, V_8 and V_{18} are the core and bypass nozzle exit velocities, P_8 and P_{18} are the corresponding exit static pressures, A_8 and A_{18} are the nozzle exit areas, and P_0 and V_0 are the ambient pressure and flight velocity, respectively. At the sea-level static condition, $V_0 = 0$.

The specific thrust is calculated as

$$ST = \frac{F_N}{\dot{m}_0} \tag{20}$$

where $\dot{m}_0$ is the total inlet air mass flow rate, given by $\dot{m}_0 = \dot{m}_c(1 + \alpha)$. The thrust-specific fuel consumption is calculated as

$$TSFC = \frac{\dot{m}_f}{F_N} \tag{21}$$

where $\dot{m}_f$ is the total fuel mass flow rate. For the baseline engine, $\dot{m}_f$ is the main-combustor fuel flow only. For the ITB-modified engine, $\dot{m}_f$ is the sum of the main-combustor and ITB fuel flow rates.

This cycle model provides the thermodynamic states and performance quantities required for the NOx emission assessment described in Section 2.3.

2.3. NOx Emission Assessment Method

A number of approaches have been developed for predicting nitrogen oxides (NOx) emissions from aircraft gas-turbine engines. At the most fundamental level, NOx formation is governed by high-temperature chemical kinetics, with the thermal NO mechanism originally described by Zeldovich forming the basis of many combustion-based models [32]. Subsequent detailed kinetic studies have refined nitrogen-chemistry mechanisms and extended them to practical combustion systems [33]. Although detailed chemical-kinetic models can provide high-fidelity predictions, their computational cost and dependence on local combustor flow-field information limit their use in system-level parametric cycle studies.

For preliminary engine design and cycle analysis, simplified empirical and semi-empirical correlations are commonly used to relate the NOx emission index to key combustor operating parameters such as combustor inlet pressure, combustor inlet temperature, fuel-air ratio, and overall combustor loading. Several cycle-parameter-based and statistical approaches have been developed

 doi:10.20944/preprints202605.1093.v1

for this purpose [6,7,22]. These models allow rapid estimation of NOx trends across a wide range of operating conditions and are useful when detailed combustor geometry, residence-time distribution, fuel-injection characteristics, and local equivalence-ratio fields are unavailable. In the present work, this type of approach is adopted because the objective is to compare relative NOx trends between the baseline and ITB-modified cycles rather than to predict certification-level emissions.

A cycle-parameter-based NOx assessment method is therefore coupled with the thermodynamic cycle model. The station-by-station cycle solution provides the local total pressures, total temperatures, and fuel-air ratios required for the emissions calculation. For the baseline configuration, NOx is evaluated for the main combustor only. For the ITB-modified configuration, the main-combustor NOx contribution and the ITB contribution are evaluated separately and then combined using a fuel-flow-weighted formulation.

2.3.1. Main-Combustor NOx Correlation

For the baseline engine, NOx formation is evaluated for the main combustor only. The main-combustor inlet state is defined at station 3, while the combustor exit state is defined at station 4. The NOx emission index of the baseline engine is therefore evaluated using the main-combustor inlet total pressure, P_{t3}, inlet total temperature, T_{t3}, and exit total temperature, T_{t4}. These quantities are calculated from the thermodynamic cycle model described in Section 2.2.

The main-combustor NOx emission index is estimated using the semi-empirical RQL-type cycle correlation [6]

$$EINOx = \left[a + b\exp\left(cT_{t,in}\right)\right]\left(\frac{P_{t,in}}{P_{ref}}\right)^{d}\exp[f_h(h_{SL}-h)]\left(\frac{\Delta T_{comb}}{\Delta T_{ref}}\right)^{TF} \quad (22)$$

where $EINOx$ is the NOx emission index, $P_{t,in}$ and $T_{t,in}$ are the combustor inlet total pressure and total temperature, respectively, h is the ambient absolute humidity, and $\Delta T_{comb} = T_{t,out} - T_{t,in}$ is the combustor total-temperature rise. The constants used in the present implementation are $a = 8.4$, $b = 0.0209$, $c = 0.0082$, $d = 0.4$, and $f_h = 19$ with $P_{ref} = 3{,}000$ kPa, $\Delta T_{ref} = 300$ K, and $h_{SL} = 0.006344$. The technology factor is set to $TF = 0$ in the present implementation. Therefore, the temperature-rise correction term becomes unity, and the calculated NOx emission index is primarily sensitive to the combustor inlet total pressure and inlet total temperature. The temperature-rise term is retained in the formulation for completeness and consistency with the selected correlation, but it is inactive in the present calculations. Consequently, the model captures the pressure-ratio sensitivity of NOx more strongly than the direct sensitivity to combustor exit temperature or HPT inlet temperature. This limitation is considered when interpreting the HPTIT sweeps, because HPTIT affects the calculated cycle state and fuel flow but does not directly enter the active part of the main-combustor NOx correlation.

2.3.2. Engineering ITB NOx Source–Sink Model

For the ITB-modified engine, the main-combustor NOx emission index is evaluated using the RQL-type correlation described in Section 2.3.1. However, the same correlation is not extrapolated directly to the ITB. The ITB operates under substantially different conditions from a conventional main combustor, including vitiated inlet gas, reduced oxygen availability, lower pressure, higher inlet temperature, shorter residence time, and different mixing characteristics. Semi-empirical NOx correlations generally remain valid only for combustor technologies and operating regimes similar to those used in their derivation, and their constants may require adaptation when applied to different combustion concepts [6]. Therefore, applying the main-combustor RQL correlation directly to the ITB would not be physically consistent.

The ITB contribution is instead represented using an engineering source-sink formulation. The source term represents new NOx formation associated with ITB fuel addition, while the sink term represents partial destruction of upstream main-combustor NOx through reburning in the secondary combustion zone. This structure is motivated by previous ITB studies indicating that NOx formed in the upstream combustor may partially dissociate or be reburned in the ITB [16,17]. The model is

 doi:10.20944/preprints202605.1093.v1

intended to provide a comparative cycle-level estimate of ITB NOx trends rather than a combustor-resolved emissions prediction.

The effective ITB NOx formation index is written as

$$EINOx_{ITB} = K_f \left(\frac{P_{t4.2}}{P_{ref}}\right)^{a_P} \left(\frac{T_{eff}}{T_{ref}}\right)^{a_T} \left(\frac{\tau_{ITB}}{\tau_{ref}}\right)^{a_\tau} \left(\frac{\phi_{ITB}}{\phi_{ref}}\right)^{a_\phi} \quad (23)$$

where $EINOx_{ITB}$ is the effective ITB NOx formation index per unit ITB fuel. This term represents newly formed NOx due to ITB fuel addition only; it does not include NOx produced upstream in the main combustor. In Equation (23), $P_{t4.2}$ is the ITB inlet total pressure, T_{eff} is the effective ITB reaction-zone temperature, τ_{ITB} is the assumed ITB residence time, and ϕ_{ITB} is a global ITB equivalence-ratio proxy. The constants K_f, P_{ref}, T_{ref}, τ_{ref}, and ϕ_{ref} are reference or scaling parameters, while a_P, a_T, a_τ, and a_ϕ are empirical engineering exponents representing the sensitivity of ITB NOx formation to pressure, effective reaction-zone temperature, residence time, and mixture strength, respectively.

The effective ITB reaction-zone temperature is approximated by

$$T_{eff} = \min(T_{t4.3} + \Delta T_{hs}, T_{eff,max}) \quad (24)$$

where $T_{t4.3}$ is the ITB exit total temperature, ΔT_{hs} is a local hot-spot allowance, and $T_{eff,max}$ is an imposed upper bound. The ITB equivalence-ratio proxy is estimated as

$$\phi_{ITB} = \frac{f_{ITB}}{FAR_{st}} \quad (25)$$

where f_{ITB} is the ITB fuel-air ratio and FAR_{st} is the stoichiometric fuel-air ratio.

The fraction of upstream NOx destroyed in the ITB is represented by the bounded reburning factor

$$R_{reburn} = R_{max}\left[1 - \exp\left(-K_r \frac{\tau_{ITB}}{\tau_{ref}} \left(\frac{T_{eff}}{T_{ref}}\right)^{b_T} \left(\frac{\phi_{ITB}}{\phi_{ref}}\right)^{b_\phi}\right)\right] \quad (26)$$

where R_{reburn} is the fraction of upstream main-combustor NOx destroyed in the ITB, R_{max} is the maximum allowable reburning fraction and K_r is the reburning strength coefficient, and b_T, and b_ϕ are empirical engineering exponents representing the sensitivity of reburning to effective reaction-zone temperature and mixture strength, respectively. The reburning factor is applied only to the NOx entering the ITB from the main combustor; it does not reduce the newly formed ITB NOx term.

The total fuel-flow-weighted NOx emission index downstream of the ITB-modified engine is then calculated as

$$EINOx_{total} = \frac{EINOx_b f_b (1 - R_{reburn}) + EINOx_{ITB} f_{ITB}}{f_b + f_{ITB}} \quad (27)$$

where $EINOx_b$ is the main-combustor emission index calculated from Equation (22), $EINOx_{ITB}$ is the effective ITB emission index calculated from Equation (23), f_b is the main-combustor fuel-air ratio, and f_{ITB} is the ITB fuel-air ratio. The first term in the numerator represents the surviving portion of main-combustor NOx after reburning in the ITB, while the second term represents new NOx formed by ITB fuel addition. For the baseline no-ITB case, $f_{ITB} = 0$ and Equation (27) reduces to

$$EINOx_{total} = EINOx_b \quad (28)$$

The engineering constants used in the ITB source-sink model are summarized in Table 5. These constants are representative engineering parameters selected for cycle-level trend assessment. They should not be interpreted as universal ITB emission constants and are not intended to replace combustor-resolved chemical-kinetic or reactor-network calculations.

 doi:10.20944/preprints202605.1093.v1

Table 5. Engineering constants used in the ITB NOx source–sink model.

Parameter group	Values
Reference conditions	$P_{ref} = 1500$ kPa; $T_{ref} = 1600$ K; $\tau_{ref} = 1.5$ ms; $\tau_{ITB} = 1.5$ ms
ITB NOx formation coefficient	$K_f = 18.0$ g/kg fuel
ITB NOx formation exponents	$a_P = 0.35$; $a_T = 4.0$; $a_\tau = 1.0$; $a_\phi = 0.30$
Effective temperature parameters	$\Delta T_{hs} = 150$ K; $T_{eff,max} = 1900$ K
Reburning parameters	$R_{\max} = 0.35$; $K_r = 0.60$; $b_T = 2.0$; $b_\phi = 0.40$
Equivalence-ratio scaling	$FAR_{st} = 0.068$; $\phi_{ref} = 0.05$

Note: The constants are representative engineering parameters selected for cycle-level trend assessment. They should not be interpreted as universal ITB emission constants and are not intended to replace combustor-resolved chemical-kinetic or reactor-network calculations.

The constants in Table 5 are selected as representative engineering parameters for a bounded cycle-level sensitivity model. They are not fitted universal ITB emission constants. The selected values are intended to produce physically interpretable comparative trends consistent with the mechanisms reported in ITB studies: formation of new NOx associated with secondary heat addition and partial reburning or dissociation of upstream main-combustor NOx in the ITB. The formation coefficient and exponents provide moderate pressure, effective-temperature, residence-time, and equivalence-ratio scaling, while the reburning term is bounded by R_{max} to prevent unrealistically complete NOx destruction. A detailed calibration of these constants requires reactor-network or combustor-resolved simulations and is identified as a future extension of the present work.

Although the adopted NOx models are expressed in terms of cycle-level variables, actual NOx formation is also affected by fuel atomization, droplet evaporation, turbulent mixing, local equivalence-ratio distribution, residence-time distribution, and flame-temperature nonuniformity. These effects are especially relevant to ITB combustor design because the ITB operates with vitiated inlet gas, short residence time, and constrained mixing length. Previous droplet-vaporization studies have shown that ambient temperature, pressure, humidity, fuel volatility, and multicomponent fuel composition can significantly influence evaporation and mixture-preparation behavior [34–38]. Such effects may become particularly important in future ITB assessments involving alternative or sustainable aviation fuels. However, they are not resolved explicitly in the present zero-dimensional cycle model.

The adopted emissions model is therefore intended for comparative trend assessment rather than certification-level emissions prediction. Accordingly, the reported NOx results should be interpreted as relative trends that indicate how ITB integration and cycle-parameter changes may influence emissions behavior, rather than as absolute certification values. This limitation is particularly important for the ITB because the additional combustor operates at lower pressure but elevated turbine-exit temperature, and its net contribution to overall NOx depends on the balance among reduced main-combustor thermal loading, upstream NOx reburning, and added downstream NOx formation.

2.4. Parametric Study Conditions and Assumptions

The parametric study is designed to compare the baseline and ITB-modified configurations under consistent modelling assumptions. Both configurations are evaluated at maximum-takeoff, sea-level static, ISA conditions using the baseline engine data and component assumptions summarized in Tables 3 and 4. The baseline engine is first solved at the reference design point, after which selected pairs of cycle parameters are varied to examine their combined influence on performance and NOx emission trends.

 doi:10.20944/preprints202605.1093.v1

For both the baseline and ITB-modified configurations, the main design variables are fan pressure ratio, bypass ratio, overall pressure ratio, and HPT inlet total temperature. For the ITB-modified configuration, the ITB exit total temperature is introduced as an additional design variable. These parameters are selected because they directly affect compressor work, turbine work distribution, fuel-air ratio, nozzle expansion, specific thrust, thrust-specific fuel consumption, and combustor inlet conditions relevant to NOx formation.

In each sweep, two design variables are varied simultaneously over prescribed ranges, while the remaining variables are held at their reference values unless otherwise stated. This approach allows the coupled influence of key cycle parameters to be examined and provides contour-type trends for identifying regions of improved thrust, reduced thrust-specific fuel consumption, or favorable NOx behavior. Although full multi-variable optimization is not performed in the present study, the two-parameter sweeps provide a systematic basis for comparing the thermodynamic and emissions response of the baseline and ITB-modified cycles.

The parametric ranges used in the cycle and emissions analysis are summarized in **Table 6**. The baseline values correspond to the reference engine and operating condition described in Section 2.2. The fan pressure ratio range is intentionally broad to examine cycle sensitivity and limiting performance trends. For the ITB-modified configuration, the ITB exit total temperature is varied over a range selected to represent moderate secondary heat addition downstream of the HPT while avoiding unrealistically high IPT inlet temperatures.

Table 6. Parametric ranges used in the thermodynamic and NOx emission analysis.

Parameter	Symbol	Reference value	Range
Fan pressure ratio	FPR	1.68	1.2 – 2.0
Bypass ratio	BPR	5.7	2.0 – 10.0
Overall pressure ratio	OPR	41.4	20.0 – 60.0
HPT inlet total temperature	Tt4	1,740 K	1,400 K – 2,000 K
ITB exit total temperature	Tt43	—	1,300 K – 1,800 K

For each case, the thermodynamic cycle model calculates the station total pressures, total temperatures, enthalpies, fuel-air ratios, turbine work distribution, nozzle exit velocities, net thrust, specific thrust, and thrust-specific fuel consumption. The NOx assessment method described in Section 2.3 is then applied using the corresponding combustor inlet and exit conditions as well as fuel-air ratios for weighting. For the baseline configuration, NOx is evaluated for the main combustor only. For the ITB-modified configuration, the main-combustor and ITB contributions are evaluated separately and then combined using the fuel-flow-weighted formulation in Equation (27).

The overall computational workflow used for the thermodynamic and NOx emission assessment is summarized in Figure 4.

The comparison between the two configurations is performed on a relative basis. The results are therefore interpreted in terms of trends and percentage changes in specific thrust, thrust-specific fuel consumption, and NOx emission index rather than as absolute certification-level performance or emissions values. This interpretation is consistent with the zero-dimensional nature of the cycle model and with the simplified NOx correlation used in the present study.

The core and bypass nozzles are modelled as convergent-only nozzles, with the exit Mach number limited to unity under choked conditions. Choking is determined from the local total-to-ambient pressure ratio and the critical pressure ratio. The exit pressure is set to ambient pressure for unchoked flow and to the critical-flow value for choked flow. The exit velocity is calculated from the total-to-static enthalpy drop, and any operating point producing a negative velocity-squared term is excluded as nonphysical.

 doi:10.20944/preprints202605.1093.v1

For the ITB-modified configuration, each prescribed ITB exit total temperature is checked against the corresponding ITB inlet total temperature obtained from the cycle solution. If the prescribed ITB exit total temperature, $T_{t4.3}$, is lower than or equal to the HPT exit/ITB inlet total temperature, $T_{t4.2}$, the corresponding operating point is excluded from the parametric results because it would not represent heat addition in the ITB.

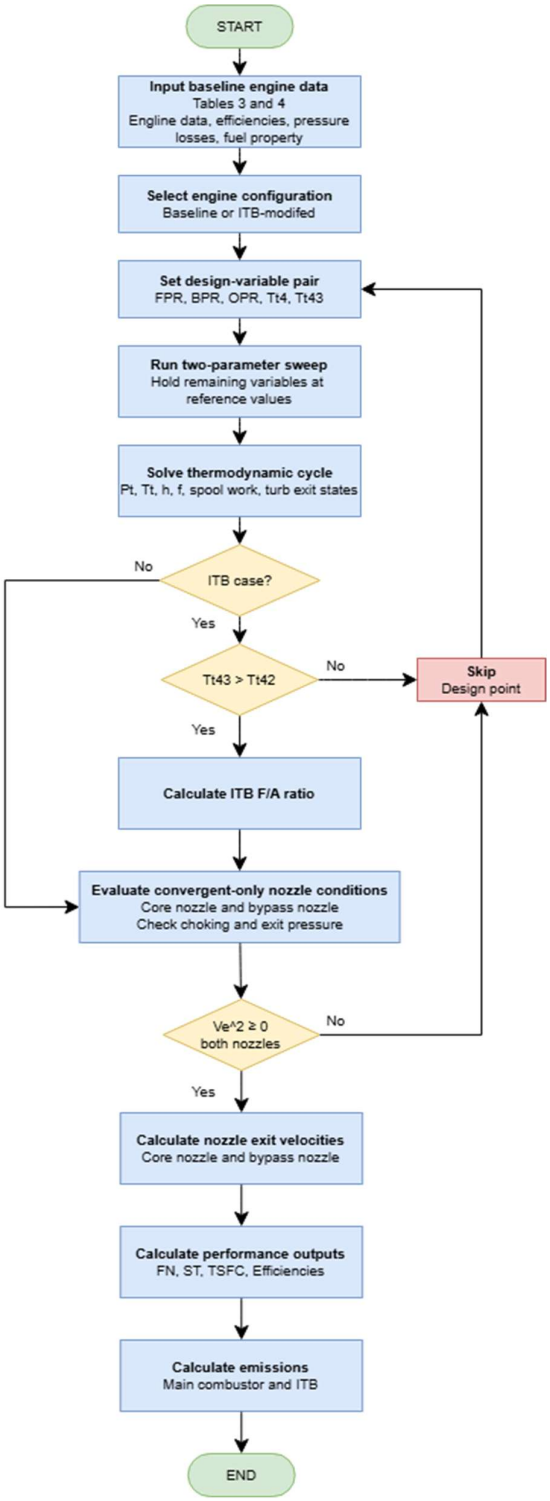

Figure 4. Computational workflow for the thermodynamic cycle analysis and NOx emission assessment of the baseline and ITB-modified turbofan configurations.

 doi:10.20944/preprints202605.1093.v1

3. Results and Discussion

The thermodynamic cycle and NOx emission assessment methods described in Section 2 were applied to the baseline and ITB-modified triple-spool turbofan configurations. The results are presented in terms of specific thrust, thrust-specific fuel consumption, and NOx emission index. The baseline configuration is first evaluated at the reference operating condition to verify the model against the rated engine data. The parametric results are then discussed to identify the influence of fan pressure ratio, bypass ratio, overall pressure ratio, HPT inlet total temperature, and ITB exit total temperature on the performance–emissions trade-off.

3.1. Baseline Model Verification

The baseline model was first evaluated at the reference maximum-takeoff, sea-level static, standard-atmosphere condition using the engine specifications and component assumptions summarized in Tables 3 and 4. The reference engine has a rated net thrust of 411.5 kN, a takeoff TSFC of 9.50 mg/(N.s), and a takeoff NOx emission index of 45.7 g/kg fuel for the RB211 Trent 892 used in the present study [28]. The corresponding reference specific thrust was derived from the ICAO-reported rated thrust and engine mass-flow rate. The calculated baseline values of specific thrust, TSFC, and EINOx were compared with these reference values to assess the consistency of the station-by-station thermodynamic cycle model and the coupled NOx correlation before applying the parametric analysis.

Table 7. Verification of the baseline cycle model at maximum-takeoff, sea-level static, ISA conditions.

Parameter	Reference value	Calculated value	Difference
TSFC (mg/(N.s))	9.50	10.26	+7.99%
Specific thrust, ST (N.s/kg)	342.92	358.66	+4.59%
EINOx (g/kg fuel)	45.7	44.28	−3.11%

The comparison in Table 7 shows that the calculated specific thrust is 4.59% higher than the ICAO-derived reference value, while the calculated TSFC is 7.99% higher than the reference value. The calculated EINOx is 3.11% lower than the ICAO takeoff emission-index value. This level of agreement is considered acceptable for the present zero-dimensional thermodynamic and emissions model, which is used primarily for comparative performance and NOx trend assessment rather than certification-level prediction.

Based on this baseline verification, the same modelling framework is applied to the parametric sweeps discussed in the following sections.

3.2. Effect of Fan Pressure Ratio and Bypass Ratio

The combined influence of fan pressure ratio and bypass ratio was examined by varying FPR and BPR while holding the remaining cycle parameters at their reference values. These two parameters mainly control the momentum split between the core and bypass streams and therefore have a direct effect on propulsive efficiency, specific thrust, and TSFC.

For the baseline configuration, increasing FPR raises the bypass-stream pressure and exit velocity, which can increase specific thrust. However, higher FPR also increases the fan work requirement, which must be supplied by the LPT and may reduce the energy available to the core nozzle. Increasing BPR generally improves propulsive efficiency by increasing the fraction of flow passing through the bypass stream, but it tends to reduce specific thrust when evaluated per unit total inlet airflow.

 doi:10.20944/preprints202605.1093.v1

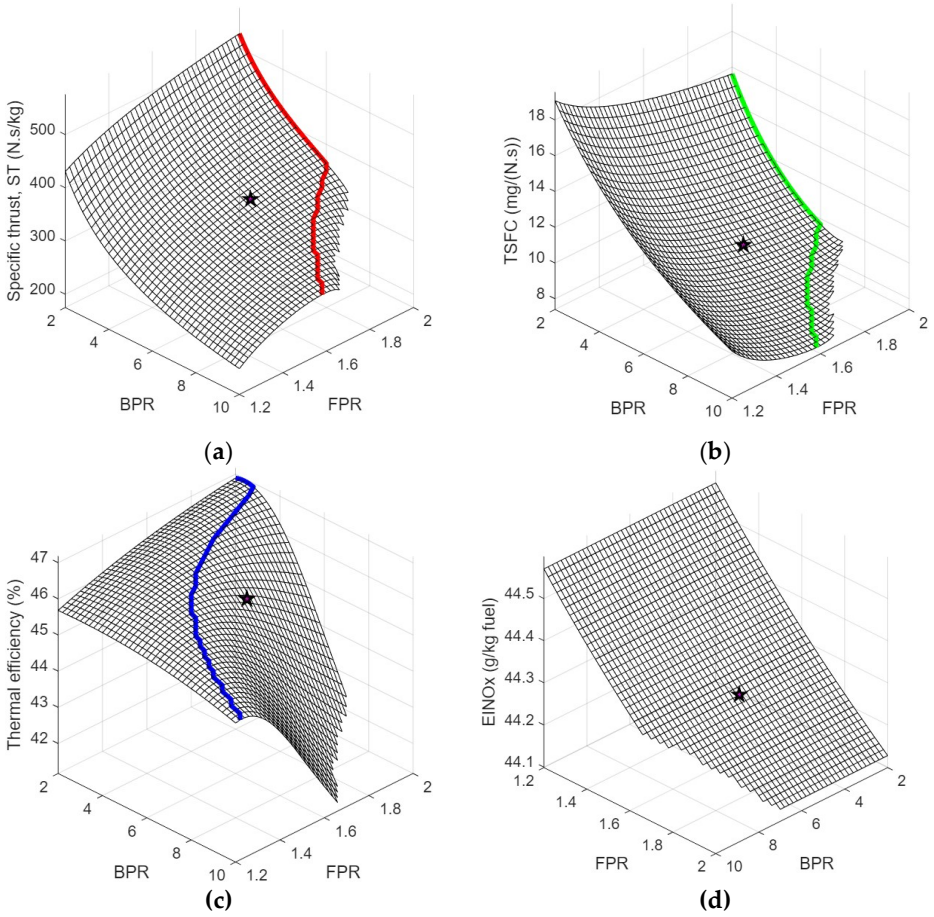

Figure 5. Effect of fan pressure ratio and bypass ratio on the baseline engine performance and emission characteristics: (a) specific thrust, (b) thrust-specific fuel consumption, (c) thermal efficiency; and (d) EINOx. In (a)–(c), the colored curves indicate the loci of maximum ST, minimum TSFC, and maximum thermal efficiency, respectively. The marker denotes the reference design point corresponding to the baseline engine.

Figure 5 summarizes the resulting performance and emission trends. The truncated regions in the response surfaces correspond to operating points that were excluded because the cycle solution became nonphysical, mainly due to invalid nozzle expansion states. Figure 5(a) shows a clear maximum-ST locus, indicating that an optimum FPR exists for each BPR. At low FPR, the bypass-stream pressure rise is insufficient to produce high jet velocity, whereas at high FPR the increased fan work demand limits further gains in specific thrust. Figure 5(b) shows a corresponding minimum-TSFC locus. For the present separate-exhaust turbofan configuration, the maximum-ST and minimum-TSFC loci occur close to each other when FPR is varied, indicating that the same fan/core work-balance mechanism controls both specific thrust and fuel consumption. Figure 5(c) shows the maximum thermal-efficiency locus, which does not necessarily coincide exactly with the ST and TSFC loci. Therefore, FPR and BPR selection remains a multi-objective cycle-design problem.

Figure 5(d) shows that EINOx varies only weakly over the FPR–BPR sweep compared with the performance parameters. The predicted EINOx is nearly insensitive to BPR because the bypass stream does not pass through the combustor. Its slight variation with FPR is attributed to indirect changes in the main-combustor inlet conditions caused by changes in fan work demand and turbine work extraction. Thus, the FPR–BPR sweep mainly affects propulsive performance, while its influence on NOx is secondary.

 doi:10.20944/preprints202605.1093.v1

3.3. Effect of Overall Pressure Ratio and HPT Inlet Temperature

The effects of overall pressure ratio (OPR) and HPT inlet total temperature (HPTIT) were examined by varying these two parameters while holding the remaining cycle parameters at their reference values. OPR and HPTIT influence compressor work, combustor inlet conditions, turbine work availability, cooling requirement, and the thermodynamic conditions associated with NOx formation.

For the baseline configuration, increasing OPR generally improves thermal efficiency over part of the design space by increasing the average temperature of heat addition. However, higher OPR also increases compressor work and raises the combustor inlet pressure and temperature, which can increase NOx formation. Increasing HPTIT increases turbine work availability and can improve specific thrust, but it also increases the main-combustor fuel-air ratio, turbine thermal loading, and the tendency for NOx formation.

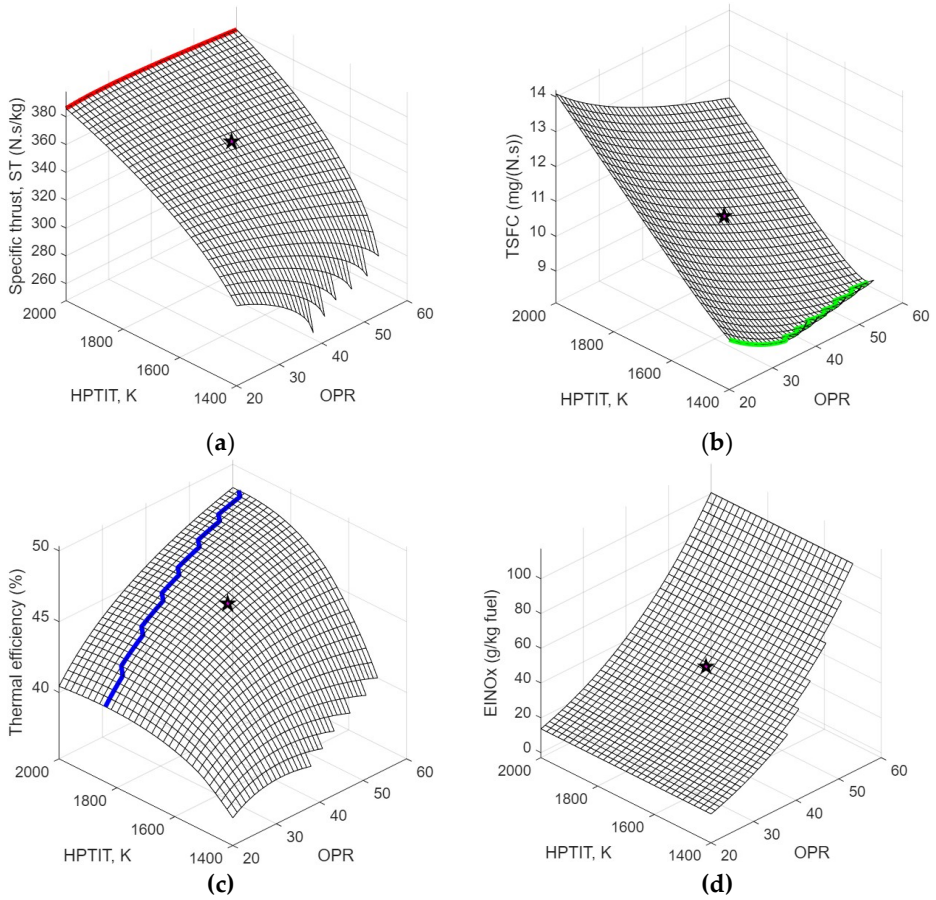

Figure 6. Effect of overall pressure ratio and HPT inlet total temperature on the baseline engine performance and emission characteristics: (a) specific thrust, (b) thrust-specific fuel consumption, (c) thermal efficiency; and (d) EINOx. In (a)–(c), the colored curves indicate the loci of maximum ST, minimum TSFC, and maximum thermal efficiency, respectively. The marker denotes the reference design point corresponding to the baseline engine.

Figure 6 summarizes the resulting OPR–HPTIT response surfaces. Figure 6(a) shows that specific thrust increases mainly with HPTIT because the higher turbine inlet temperature increases the available turbine work and exhaust kinetic energy. The maximum-ST locus occurs near the upper HPTIT boundary, indicating that ST is primarily temperature-driven within the investigated range. Figure 6(b) shows a clear minimum-TSFC locus. At low HPTIT, the cycle has limited specific work, whereas at high HPTIT the additional fuel input becomes dominant; therefore, minimum TSFC

 doi:10.20944/preprints202605.1093.v1

occurs at an intermediate combination of OPR and HPTIT. Figure 6(c) shows a maximum thermal-efficiency locus, reflecting the competing effects of pressure-ratio benefit, compressor work, turbine work extraction, and cooling losses.

Figure 6(d) shows that EINOx increases mainly with OPR, while its variation with HPTIT at fixed OPR is weak. This trend is consistent with the adopted NOx correlation, which relates the emission index primarily to the main-combustor inlet pressure and temperature. Increasing OPR raises both P_{t3} and T_{t3}, thereby increasing the predicted EINOx. In contrast, HPTIT mainly affects the required fuel-air ratio and turbine work availability, but it does not directly enter the NOx correlation except through secondary cycle-coupling effects. Therefore, the present model captures the pressure-ratio sensitivity of NOx more strongly than the flame-temperature or combustor-exit-temperature sensitivity.

Overall, the OPR–HPTIT sweep highlights the trade-off between performance improvement and emissions. Higher HPTIT can increase specific thrust, while increasing OPR can improve thermal efficiency over part of the design space. However, higher OPR also intensifies the main-combustor inlet pressure and temperature, leading to higher predicted EINOx. Therefore, OPR and HPTIT selection must balance specific thrust, TSFC, thermal efficiency, turbine thermal loading, and NOx emissions, while recognizing that the present NOx correlation is more sensitive to combustor inlet conditions than to HPTIT directly.

3.4. Effect of ITB Exit Temperature

The effect of ITB exit total temperature, $T_{t4.3}$, was examined to assess how secondary heat addition between the HPT and IPT affects the thermodynamic performance and NOx emission characteristics of the ITB-modified triple-spool turbofan cycle. In this configuration, the ITB is located downstream of the HPT and upstream of the IPT. Increasing $T_{t4.3}$ therefore raises the thermal energy available to the IPT and LPT system without increasing the main-combustor exit temperature, T_{t4}. This allows the influence of secondary heat addition to be examined separately from the thermal loading imposed on the HPT.

For this sweep, $T_{t4.3}$ was varied over the prescribed ITB operating range, while the remaining reference cycle parameters were held fixed unless otherwise stated. At each operating point, the ITB fuel-air ratio, f_{ITB}, was calculated from the required temperature rise between stations 4.2 and 4.3. The main-combustor NOx emission index was evaluated using the RQL-type cycle correlation, while the ITB contribution was evaluated using the engineering source–sink model described in Section 2.3. The two contributions were then combined using the fuel-flow-weighted formulation.

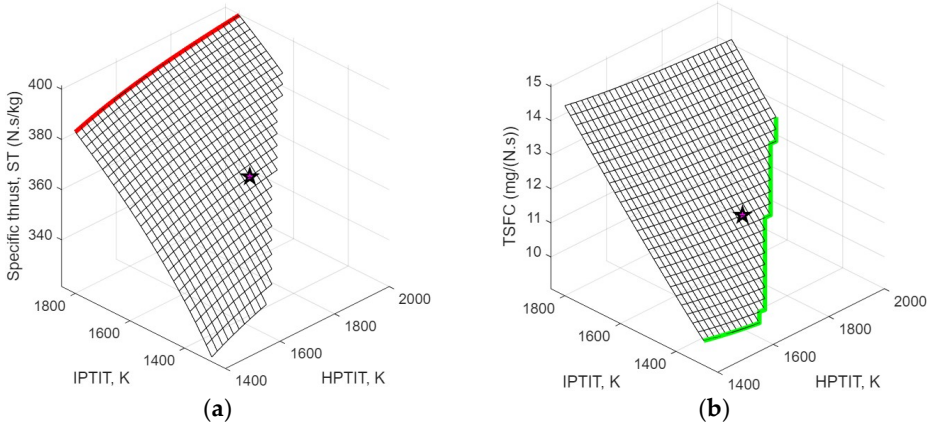

(**a**) (**b**)

 doi:10.20944/preprints202605.1093.v1

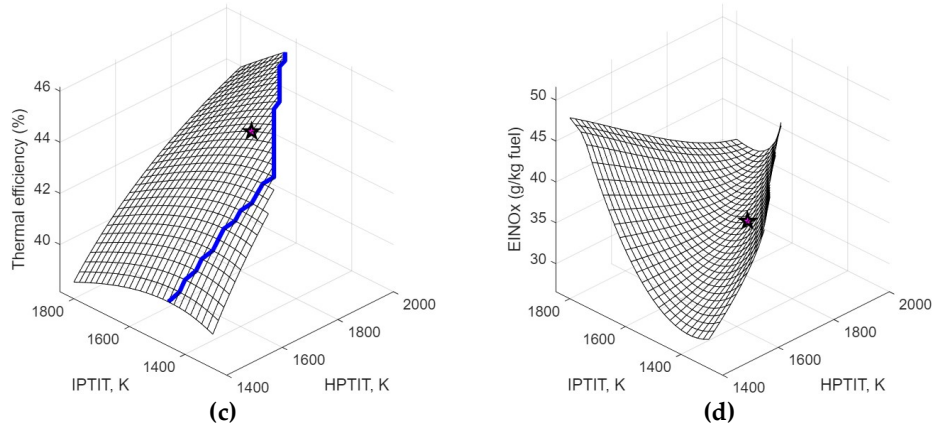

Figure 7. Effect of HPT inlet total temperature (HPTIT, T_{t4}) and IPT inlet total temperature (IPTIT, $T_{t4.3}$) on the ITB-modified engine: (a) specific thrust, (b) thrust-specific fuel consumption, (c) thermal efficiency, and (d) total fuel-flow-weighted EINOx predicted using the engineering ITB source–sink NOx model. In (a)–(c), the colored curves indicate the loci of maximum ST, minimum TSFC, and maximum thermal efficiency, respectively. The marker denotes the selected ITB operating point. Blank or truncated regions indicate excluded nonphysical operating points, including cases where the prescribed ITB exit total temperature does not exceed the HPT-exit/ITB-inlet total temperature.

Figure 7 presents the response surfaces obtained by varying HPTIT and IPTIT for the ITB-modified engine. Figure 7(a) shows that specific thrust increases mainly with IPTIT, while its sensitivity to HPTIT is comparatively weaker over much of the investigated range. This indicates that secondary heat addition through the ITB is effective in increasing the energy available to the downstream turbine stages and core nozzle. The maximum-ST locus lies near the upper IPTIT boundary, showing that the highest specific thrust is obtained when the ITB exit temperature is increased within the feasible design space.

Figure 7(b) shows that TSFC increases with increasing IPTIT because the additional thrust is obtained through extra ITB fuel addition. The minimum-TSFC locus occurs near the lower feasible IPTIT boundary, indicating that moderate ITB heat addition is more favorable from a fuel-consumption perspective. Therefore, the ST and TSFC trends reveal a clear thrust–fuel-consumption trade-off: increasing IPTIT improves specific thrust but penalizes TSFC.

Figure 7(c) shows that thermal efficiency increases with HPTIT and IPTIT over part of the design space, but the maximum-efficiency locus does not coincide exactly with either the maximum-ST or minimum-TSFC locus. This reflects the competing effects of increased heat addition, turbine work availability, cooling requirement, and useful exhaust power. Thus, the thermally most efficient operating region is not necessarily the same as the region of highest thrust or lowest fuel consumption.

Figure 7(d) shows a non-monotonic EINOx response predicted by the engineering ITB source–sink NOx model. A low-EINOx region appears at moderate IPTIT and HPTIT, where the combined effects of fuel-flow weighting and partial reburning of upstream main-combustor NOx offset the new NOx formed in the ITB. At higher IPTIT and HPTIT, EINOx increases as the ITB NOx formation term and main-combustor severity become more important. This behavior indicates that ITB operation can provide an emission benefit only within a limited operating range; excessive secondary heat addition can reverse this benefit.

Overall, Figure 7 highlights the main performance–emissions trade-off associated with ITB operation. Increasing IPTIT provides additional thrust capability, but this comes with a TSFC penalty and a possible increase in EINOx at high temperature levels. The favorable operating region is therefore not located at the maximum-temperature boundary, but rather at intermediate IPTIT values where acceptable thrust enhancement is obtained while maintaining lower fuel-flow-weighted EINOx.

 doi:10.20944/preprints202605.1093.v1

To quantify the trends shown in Figure 7, the selected ITB operating point is compared with the verified baseline case in Table 8. This point corresponds to HPTIT = 1740 K and IPTIT = 1500 K. It is selected as a representative moderate-ITB case because it preserves the baseline HPTIT while placing IPTIT within the favorable low-EINOx region of the response surface. It is not intended to represent a global optimum over the full design space.

Table 8. Performance and NOx comparison between the verified baseline engine and the selected ITB operating point at HPTIT = 1740 K and IPTIT = 1500 K.

Case	HPTIT, K	IPTIT, K	ST, N.s/kg	TSFC, mg/(N.s)	Thermal efficiency, %	EINOx, g/kg fuel
Baseline	1740	—	358.66	10.26	45.65	44.28
Selected ITB case	1740	1500	365.75	11.27	44.48	35.41
Change	—	—	+1.98%	+9.84%	−2.56%	−20.03%

Overall, the HPTIT–IPTIT sweep shows that ITB operation introduces a clear performance–emissions trade-off. Moderate ITB heat addition can increase specific thrust and reduce the predicted fuel-flow-weighted EINOx, but this benefit is accompanied by higher TSFC and lower thermal efficiency. Therefore, ITB exit temperature should be treated as a coupled cycle-design variable rather than simply as a thrust-augmentation parameter.

4. Conclusions

This study assessed the thermodynamic performance and NOx emission behavior of a triple-spool, separate-exhaust turbofan engine modified with an interstage turbine burner. The baseline engine was first verified against publicly available Trent 892 reference data at maximum-takeoff, sea-level static, ISA conditions. The calculated baseline specific thrust, TSFC, and EINOx showed acceptable agreement with the reference values, supporting the use of the model for comparative cycle-level trend assessment rather than certification-level prediction.

The FPR–BPR sweep showed that fan pressure ratio and bypass ratio mainly affect propulsive performance. A clear optimum-FPR trend was observed for specific thrust and TSFC, reflecting the balance between bypass-stream momentum increase and the fan work extracted through the low-pressure turbine. The corresponding EINOx variation was weak because the bypass stream does not pass through the combustor and because the main combustor inlet conditions changed only indirectly over this sweep.

The OPR–HPTIT sweep showed that increasing OPR increases the predicted EINOx mainly through its effect on main-combustor inlet pressure and temperature. In contrast, HPTIT had a weaker direct effect on EINOx in the present implementation because the active part of the adopted main-combustor NOx correlation depends primarily on combustor inlet conditions. This result highlights the importance of interpreting the NOx trends in relation to the structure and limitations of the selected cycle-level correlation.

For the ITB-modified configuration, the HPTIT–IPTIT sweep showed that secondary heat addition can increase specific thrust by raising the energy available to the downstream turbine stages and core nozzle. However, this thrust benefit is accompanied by increased ITB fuel flow, which raises TSFC and can reduce thermal efficiency. The selected ITB operating point increased specific thrust by 1.98% relative to the verified baseline case, but increased TSFC by 9.84% and reduced thermal efficiency by 2.56%.

The engineering ITB source–sink NOx model predicted a non-monotonic EINOx response. Moderate ITB heat addition reduced the total fuel-flow-weighted EINOx because the combined effects of fuel-flow weighting and partial reburning of upstream main-combustor NOx outweighed the new NOx formed in the ITB. Using the adopted engineering ITB source–sink model, the selected

 doi:10.20944/preprints202605.1093.v1

ITB operating point reduces the predicted fuel-flow-weighted EINOx by 20.03% relative to the baseline case. However, higher IPTIT levels increased the ITB NOx formation contribution and could reduce or reverse this emissions benefit.

Overall, the results indicate that ITB integration should not be evaluated solely as a thrust-augmentation method. Its benefit depends on the coupled balance among specific thrust, TSFC, thermal efficiency, turbine thermal loading, and fuel-flow-weighted NOx emissions. The most favorable operating region is not necessarily located at the maximum IPTIT boundary, but rather at moderate ITB exit temperatures where useful thrust enhancement can be obtained while maintaining lower predicted EINOx. Future work should focus on validating the engineering ITB NOx model using reactor-network or combustor-resolved simulations, extending the analysis to off-design operation, and examining ITB temperature scheduling for thrust and emissions control across the flight envelope.

Author Contributions: The author confirms sole responsibility for the conceptualization, methodology, software implementation, validation, formal analysis, investigation, data curation, visualization, writing—original draft preparation, and writing—review and editing of this manuscript. The author has read and agreed to the published version of the manuscript.

Funding: This research received no external funding.

Data Availability Statement: The public engine data used in this study are available from the cited EASA and ICAO sources. The calculated data generated during the present study are available from the corresponding author upon reasonable request.

Acknowledgments: The author acknowledges Hariharan Ravichandran for his contribution to the earlier conference study on the triple-spool turbofan cycle analysis with an interstage turbine burner, which provided background motivation for the present work. The author also acknowledges the use of AI-assisted language tools during manuscript preparation for language refinement, structural organization, MATLAB code support, and editorial refinement. All technical content, model formulation, numerical results, figures, interpretations, and references were reviewed, verified, and approved by the author, who takes full responsibility for the final content of the manuscript.

Conflicts of Interest: The author declares no conflict of interest.

Abbreviations

The following abbreviations are used in this manuscript:

BPR	Bypass ratio
EASA	European Union Aviation Safety Agency
EINOx	NOx emission index
FAR	Fuel-air ratio
FPR	Fan pressure ratio
HPC	High-pressure compressor
HPS	High-pressure spool
HPT	High-pressure turbine
HPTIT	High-pressure turbine inlet temperature
ICAO	International Civil Aviation Organization
IPC	Intermediate-pressure compressor
IPS	Intermediate-pressure spool
IPT	Intermediate-pressure turbine
IPTIT	Intermediate-pressure turbine inlet temperature
ISA	International Standard Atmosphere
ITB	Interstage turbine burner
LHV	Lower heating value
LPS	Low-pressure spool
LPT	Low-pressure turbine

 doi:10.20944/preprints202605.1093.v1

NOx	Nitrogen oxides
OPR	Overall pressure ratio
RPM	Revolutions per minute
ST	Specific thrust
TSFC	Thrust-specific fuel consumption

References

1. Koff, B.L. Gas Turbine Technology Evolution: A Designer's Perspective. *J. Propuls. Power* **2004**, *20*, 577–595, doi:10.2514/1.4361.
2. Parker, R.; Fedder, G. Aircraft Engines: A Proud Heritage and an Exciting Future. *Aeronaut. J.* **2016**, *120*, 131–169, doi:10.1017/aer.2015.6.
3. International Civil Aviation Organization (ICAO) *Skyward Action: Realizing Aviation's Sustainable Future*; ICAO Environmental Report; International Civil Aviation Organization (ICAO): Montreal, Canada, 2025;
4. European Commission. Directorate General for Research and Innovation.; European Commission. Directorate General for Mobility and Transport. *Flightpath 2050: Europe's Vision for Aviation: Maintaining Global Leadership and Serving Society's Needs.*; Publications Office: LU, 2012;
5. Intergovernmental Panel on Climate Change (IPCC) *Aviation and the Global Atmosphere*; IPCC Special Report; Cambridge University Press: Cambridge, UK, 1999;
6. Kyprianidis, K.G.; Nalianda, D.; Dahlquist, E. A NOx Emissions Correlation for Modern RQL Combustors. *Energy Procedia* **2015**, *75*, 2323–2330, doi:10.1016/j.egypro.2015.07.433.
7. Hasanovic, A.; Sarikaya, M.A. *NOx Emissions of the 50 Most Used Engines for Passenger Aircraft*; Hamburg University of Applied Sciences (HAW Hamburg): Hamburg, Germany, 2025;
8. Sirignano, W.A.; Liu, F. Performance Increases for Gas-Turbine Engines Through Combustion Inside the Turbine. *J. Propuls. Power* **1999**, *15*, 111–118, doi:10.2514/2.5398.
9. Liu, F.; Sirignano, W.A. Turbojet and Turbofan Engine Performance Increases Through Turbine Burners. *J. Propuls. Power* **2001**, *17*, 695–705, doi:https://doi.org/10.2514/2.5797.
10. Chen, G.; Hoffman, M.A.; Davis, R.L. Gas-Turbine Performance Improvements Through the Use of Multiple Turbine Interstage Burners. *J. Propuls. Power* **2004**, *20*, 828–834, doi:10.2514/1.2886.
11. Liew, K.H.; Urip, E.; Yang, S.L. Parametric Cycle Analysis of a Turbofan Engine with an Interstage Turbine Burner. *J. Propuls. Power* **2005**, *21*, 546–551, doi:10.2514/1.2546.
12. K.H. Liew,; E. Urip; S.L. Yang; Y.K. Siow; C.J. Marek *Parametric On-Design Cycle Analysis for a Separate-Exhaust Turbofan Engine With Interstage Turbine Burner*; NASA Glenn Research Center, 2005;
13. K. H. Liew; E. Urip; S. L. Yang; J. D. Mattingly; C. J. Marek *Performance (Off-Design) Cycle Analysis for a Turbofan Engine With Interstage Turbine Burner*; NASA Glenn Research Center, 2005;
14. Liew, K.H.; Urip, E.; Yang, S.; Mattingly, J.; Marek, C. *Performance Cycle Analysis of a Two-Spool, Separate-Exhaust Turbofan with Interstage Turbine Burner*; NASA Glenn Research Center: Fort Lauderdale, Florida, 2004;
15. Jakubowski, R. Analysis of Turbofan Engine Design Modification to Add Inter-Turbine Combustor. *J. KONES Powertrain Transp.* **2015**, *22*, 75–82, doi:10.5604/12314005.1165974.
16. Yin, F.; Rao, A.G. Performance Analysis of an Aero Engine with Inter-Stage Turbine Burner. *Aeronaut. J.* **2017**, *121*, 1605–1626, doi:10.1017/aer.2017.93.
17. Yin, F.; Rao, A.G. A Review of Gas Turbine Engine with Inter-Stage Turbine Burner. *Prog. Aerosp. Sci.* **2020**, *121*, 100695, doi:10.1016/j.paerosci.2020.100695.
18. Zheng, H.; Yu, X.; Tang, H. Analysis of Overall Thermodynamic Performance for Aero-Engine Using Turbine Internal Burner Technology. *J. Phys. Conf. Ser.* **2025**, *2965*, 012009, doi:10.1088/1742-6596/2965/1/012009.
19. Ji, Z.; Qin, J.; Cheng, K.; Liu, H.; Zhang, S.; Dong, P. Performance Evaluation of a Turbojet Engine Integrated with Interstage Turbine Burner and Solid Oxide Fuel Cell. *Energy* **2019**, *168*, 702–711, doi:10.1016/j.energy.2018.11.088.
20. Conrad, M.M. Integration of an Inter Turbine Burner to a Jet Turbine Engine. Master of Science in Aeronautical Engineering, Air Force Institute of Technology: Wright-Patterson Air Force Base, Ohio, 2013.

 doi:10.20944/preprints202605.1093.v1

21. Zhang, H.; Luo, G.; Guan, L.; Zeng, J. Performance Investigation on an Ultra-Compact Interstage Turbine Burner with Trapped-Vortex Slot Inlet. *J. Phys. Conf. Ser.* **2017**, *916*, 012013, doi:10.1088/1742-6596/916/1/012013.
22. Shakariyants, S.A. Generic Methods for Aero-Engine Exhaust Emission Prediction. PhD Thesis, Delft University of Technology: Delft, Netherlands, 2008.
23. Kafafy, R.; Ravichandran, H. A Parametric Cycle Analysis of a Triple-Spool, Separate-Exhaust, Turbofan Engine with Inter-Stage Turbine Burners. In Proceedings of the Advances in Transdisciplinary Engineering; Lei, X., Ed.; IOS Press, March 3 2026.
24. Rolls-Royce plc *The Jet Engine*; 5th ed.; Rolls-Royce plc: Derby, UK, 2015; ISBN 978-1-119-06599-9.
25. Mattingly, J.D.; Boyer, K.M.; Ohain, H. von *Elements of Propulsion: Gas Turbines and Rockets*; AIAA education series; Second edition.; American Institute of Aeronautics and Astronautics, Inc: Reston, VA, 2016; ISBN 978-1-62410-371-1.
26. Farokhi, S. *Aircraft Propulsion: Cleaner, Leaner, and Greener*; Third edition.; Wiley: Hoboken, 2022; ISBN 978-1-119-71864-2.
27. European Union Aviation Safety Agency (EASA) *EASA Type-Certificate Data Sheet EASA E.047 RB211 Trent 800 Series Engines*; European Union Aviation Safety Agency, 2019;
28. International Civil Aviation Organization (ICAO) ICAO Aircraft Engine Emissions Databank 2025.
29. Gordon, S.; McBride, B.J. *Computer Program for Calculation of Complex Chemical Equilibrium Compositions, Rocket Performance, Incident and Reflected Shocks, and Chapman-Jouguet Detonations*; National Aeronautics and Space Administration, Glenn Research Center, 1978;
30. McBride, B.J.; Zehe, M.J.; Gordon, S. *NASA Glenn Coefficients for Calculating Thermodynamic Properties*; National Aeronautics and Space Administration, Glenn Research Center, 2002;
31. Zehe, M.J.; Gordon, S.; McBride, B.J. *CAP -A Computer Code for Generating Tabular Thermodynamic Functions from NASA Lewis Coefficients*; National Aeronautics and Space Administration, Glenn Research Center, 2002;
32. Zeldovich, Y.B. The Oxidation of Nitrogen in Combustion and Explosions. In *Selected Works of Yakov Borisovich Zeldovich, Volume I*; Sunyaev, R.A., Ed.; Princeton University Press, 1992 ISBN 978-1-4008-6297-9.
33. Glarborg, P.; Miller, J.A.; Ruscic, B.; Klippenstein, S.J. Modeling Nitrogen Chemistry in Combustion. *Prog. Energy Combust. Sci.* **2018**, *67*, 31–68, doi:10.1016/j.pecs.2018.01.002.
34. Abramzon, B.; Sirignano, W.A. Droplet Vaporization Model for Spray Combustion Calculations. *Int. J. Heat Mass Transf.* **1989**, *32*, 1605–1618, doi:10.1016/0017-9310(89)90043-4.
35. Ghassemi, H.; Baek, S.W.; Khan, Q.S. Experimental Study on Binary Droplet Evaporation at Elevated Pressures and Temperatures. *Combust. Sci. Technol.* **2006**, *178*, 1031–1053, doi:10.1080/00102200500296697.
36. Eyice, D.K.; Renoux, G.; Halter, F.; Yozgatlıgil, A.; Gökalp, I.; Chauveau, C. Vaporization Characteristics of an Isolated Ethanol Droplet at Flame Conditions. *At. Sprays* **2022**, *32*, 79–94, doi:10.1615/AtomizSpr.2022041118.
37. Saharin, S.; Lefort, B.; Morin, C.; Chauveau, C.; Le Moyne, L.; Kafafy, R. Vaporization Characteristics of Ethanol Droplets: Influence of the Environment Humidity. In Proceedings of the Volume 1: Aircraft Engine; Ceramics; Coal, Biomass and Alternative Fuels; Wind Turbine Technology; ASMEDC: Vancouver, British Columbia, Canada, January 1 2011; pp. 669–676.
38. Saharin, S.; Lefort, B.; Morin, C.; Chauveau, C.; Le Moyne, L.; Kafafy, R. Vaporization Characteristics of Ethanol and 1-Propanol Droplets at High Temperatures. *At. Sprays* **2012**, *22*, 207–226, doi:10.1615/AtomizSpr.2012005061.